17th International Conference on Space Operations, Dubai, United Arab Emirates, 6 - 10 March 2023.

SpaceOps-2023, ID # 515

Autonomous tracking of Resident Space Objects using multiple ground-based Electro-Optical sensors

Khaja Faisal Hussain[a]*, Kathiravan Thangavel[b], Alessandro Gardi[a,b], Roberto Sabatini[a,b]

[a] *Department of Aerospace Engineering, Khalifa University of Science and Technology, Abu Dhabi, UAE,* 100060970@ku.ac.ae , alessandro.gardi@ku.ac.ae, roberto.sabatini@ku.ac.ae
[b] *Sir Lawrence Wackett Defence & Aerospace Centre, RMIT University, Melbourne, VIC, 3083, Australia* kathiravan.thangavel@student.rmit.edu.au
* Corresponding Author 100060970@ku.ac.ae

Abstract

Space debris has increased significantly in the past decade. Despite growing awareness of the orbital debris problem, recent developments such as growth in the availability of small launch vehicles, and particularly large-scale satellite constellation deployments in Low Earth Orbits (LEO), are dramatically increasing on-orbit congestion. With no active space debris removal solutions, tracking and catalogue maintenance of Resident Space Objects (RSO) is pivotal in the context of Space Domain Awareness (SDA) for Space Traffic Management (STM). This paper presents a novel and computationally efficient approach to on-orbit position uncertainty generation using ground-based Electro-Optical (EO) sensors. The proposed method combines the navigation errors of the host platform and tracking errors of the intruder (RSO), to determine the combined avoidance volume for multi-platform Separation Assurance (SA). This data is shared in a Distributed Satellite Systems (DSS) network and the spacecraft with identified high risk of collision perform appropriate avoidance maneuvers, which can take place both in the orbital plane and out-of-plane. A simulation case study is performed where RSO are tracked using a ground network of passive infrared EO sensors and, based on collision threat information uplinked to the DSS, the onboard satellite systems plan and execute an orbit-raising maneuver for debris collision avoidance using a Particle Swarm Optimization (PSO) algorithm, which accounts for all applicable astrodynamic perturbations in LEO. The simulation results corroborate the validity of the proposed SA approach in the context of DSS operations.

Keywords: Distributed Satellite Systems, Space Domain Awareness, Space Traffic Management, Resident Space Objects, Trusted Autonomous Satellite Operations (TASO),

1. Introduction

Space debris, also referred to as Resident Space Objects (RSO) are non-functional, man-made objects in outer space including large objects of several meters in size like damaged satellites, upper stages of launch vehicles and other centimeter and millimetre-sized fragments including paint flakes, and solid rocket motor slag or dust resulting from explosions and collisions [1]. Consequently, most space debris is found in geocentric orbits with altitudes ranging from 200 to 50,000 km. Evidently, from optical surveys, space debris appears as fast-moving objects with angular velocities more than 1,000 arc seconds per second. At these speeds, even a small screw or a nail can destroy the ISS (International Space Station) into pieces. Space debris poses a formidable hazard to the operating spacecrafts and the largest inhabited space station ISS is the most vulnerable target. Fig.1 illustrates the current space domain scenario. Recently published statistics by ESA [2] states that there were in total 6170 rocket launches since 1957 that put 12480 satellites into orbit (excluding failures). Currently, there are 36500 objects greater than 10cm, 1000000 objects ranging from 1cm-10cm and 330million objects in the range of 1mm-1cm. The collision between Iridium 33 and Cosmos 2251, along with the destruction of the Fengyun-1C weather satellite by an Anti-Satellite (ASAT) missile test in 2007 created a significant number of debris. The ASAT test gave rise to more than 3,500 pieces of debris, most of which are still orbiting in the ISS's orbital region. The development of the RSO population by object type is emphasized in Fig. 2, which also underlines the significant portion of RSO produced because of collision or fragmentation events. It is possible to predict the collision probability of large orbiting objects (>10 cm) with reasonable accuracy based on data obtained through traditional tracking hardware, allowing a satellite to maneuver, thereby reducing collision possibilities. However, the same cannot be concluded for objects that lie in cm-mm range or even smaller, which are challenging to track using conventional ground-based sensors. Collisions with small, undetectable debris and micro-meteorites are responsible for several abnormalities and continuous performance degradation (e.g., solar cell

deterioration) in satellite performance there by resulting in increase in non-functional satellites further worsening the space situation and jeopardizing national security imperatives.

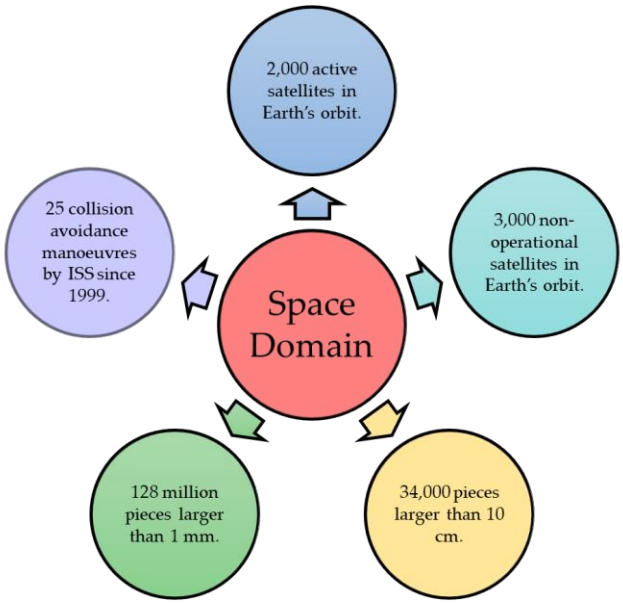

Fig. 1. The present space domain scenario.

Commercial operations have outpaced government and military operations in recent years due to the launch of large "New Space" constellations like Star-link and One-Web. Due to the proliferation of space activities, space debris impose a formidable threat making it imperative for the spacecraft operators to have better awareness of existing RSOs (Resident Space Objects). However, despite the proliferation of space activity, the ability of the space actors to track and regulate space objects is termed as Space Traffic Management (STM) [3] and as a part of this process, RSOs need to be tracked, cataloged, and the probability of accidental collisions must be analyzed and calculated to prevent any further collisions. This critical task is referred to as Space Domain Awareness (SDA) or Space Situational Awareness (SSA).

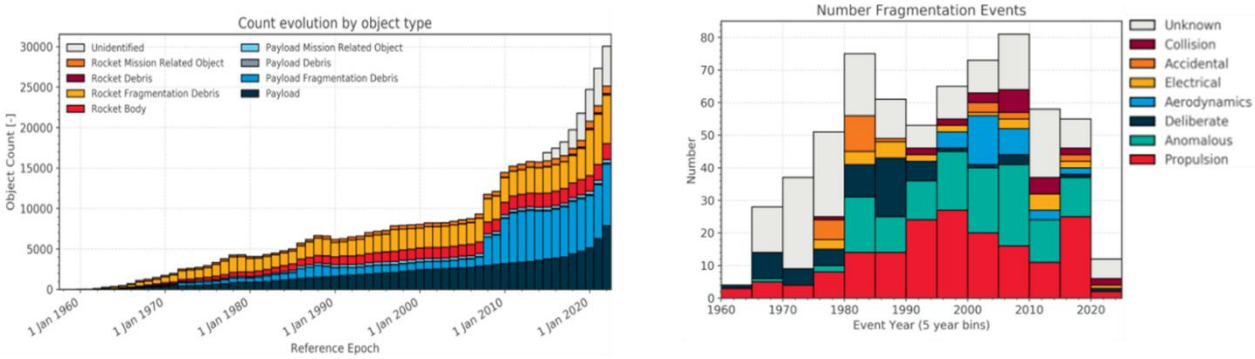

(a) **(b)**

Fig. 2. (a) RSO population evolution by object type, (b) Number of fragmentation events till 2020 [2].

It is customary for the US Department of Defense to perform these tasks through a network of ground-based observation facilities known as the Space Surveillance Network (SSN) [4]. Additionally, various other ground based surveillance systems contribute towards SSA [5]. Table 1 provides a summary of major ground-based systems and the time frame during which they were introduced. As an alternative to radar, optical observation has become increasingly

popular in space debris observation because of its ability to observe objects from a distance and cost efficiency. Several countries have already conducted optical space debris observation [6]–[10].

Table 1. Major ground-based space surveillance systems.

USA		***Russia***		***Japan***		***Europe***	
System	***Year***	***System***	***Year***	***System***	***Year***	***System***	***Year***
Thule radar	1943	Dnepr radar	1963	BSGC	2002	GRAVES (France)	2005
Eglin radar	1969	Dunay-3U radar	1968	KSGC	2004	TIRA (Germany)	2009
GEODSS	1980	Daryal radar	1984				
SST	2011	Don-2N radar	1996				
Space fence	2020	Okno optical complex	1997				
		Krona system	2008				

In this paper a non-cooperative RSO tracking scenario is analyzed [11], in which multiple ground-based Electro-Optical (EO) sensors track RSO subject to specific measurement errors. These tracking errors (3-sigma values) are combined to the host DSS spacecraft positioning errors in space and time to form the total 3-sigma Collision Probability Volume (CPV). The CPV is then utilized to plan and execute Separation Assurance (SA) maneuvers [12].

2. Multi-sensor tracking scenario

To estimate the position of an RSO in 3D, the position of the sensors (x_1, y_1, z_1), (x_2, y_2, z_2) and Line of Sight (LOS) azimuth (θ_1, θ_2) and elevation (φ_1, φ_2) pointing angles from the sensor to RSO is necessary. Inaccurate knowledge of these parameters will ultimately lead to an inaccurate RSO position co-ordinates. Additionally, the sensor-target-sensor geometry influences the relationship between measurement error and errors in the predicted target location, where a sensor-target-sensor separation of 90° results in the lowest error sensitivity, while a sensor separation of 0° or 180° results in impossible solutions (as seen from the target). To define the triangulation problem, we need to define the positions of the sensors and the RSO in a right-handed coordinate system as illustrated in Fig.3a. The x and y axis forms the horizontal plane and z-axis pointing out of the plane vertically with Earth's center as the origin. θ_1 and θ_2 are the azimuth angles of the corresponding sensors measured clockwise measured from the positive y-axis towards positive x axis. The corresponding elevation angles are denoted by φ_1 and φ_2 varying from 0^0 to 90^0 pointing vertically. The horizontal ranges from the x-y components of the sensor to the x and y components of the RSO are denoted by r_1 and r_2 respectively. The separation angle θ_{sep} is measured from sensor 1 through RSO to sensor 2.

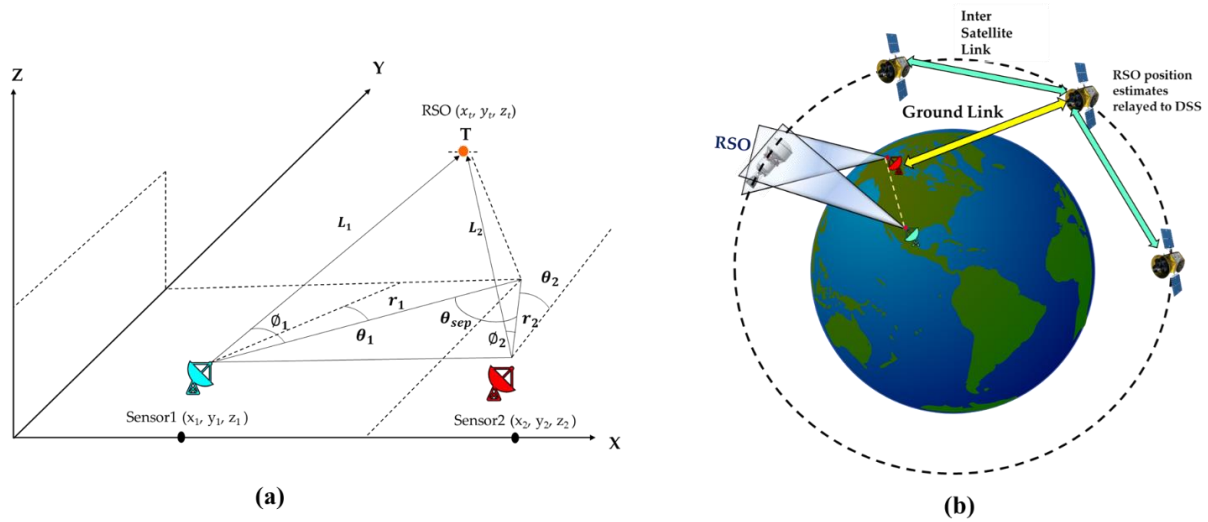

Fig. 3. Multi-sensor tracking and inter-satellite links.

As illustrated in Fig.3b two ground based EO sensors track the RSO simultaneously and share the estimated RSO position data with a Distributed Satellite System (DSS) constellation through a network [13]–[16]. For the assumed DSS constellation the following assumptions are adopted: (1) the DSS assets are placed in a nearly circular Low Earth Orbit (LEO) orbit at an altitude of 450 km to carry out earth observation activities; (2) the participating spacecrafts are equipped with GPS for positioning and navigation that provide full set of navigation data; (3) the estimated RSO position from ground-based sensors is relayed to the DSS assets to ensure their safety; and (4) the participating spacecrafts share their position information and the RSO position estimates with other satellites using Inter-Satellite Links (ISL). The proposed autonomous navigation system comprises of the following components:

- **Navigation hardware** comprises of the state-of-the-art GPS to obtain a full set of navigation data comprising of the DSS satellites positions, velocities, and attitude rates.
- **Tracking hardware** comprises of ground based EO sensors that track the RSO by simultaneous optical measurements.
- The obtained data from the hardware is used as inputs by the **On-Board System (OBS)** to obtain the RSO position estimates, error measurement budget and to generate the uncertainty ellipsoids.
- The **navigation and guidance system** exploits the data generated by the OBS for trajectory planning and optimization to generate the steering commands.
- **Actuators** use the steering commands to perform the collision avoidance maneuvers in order to avoid a collision with the RSO.

Figure 4 illustrates the individual segments of the tracking system architecture.

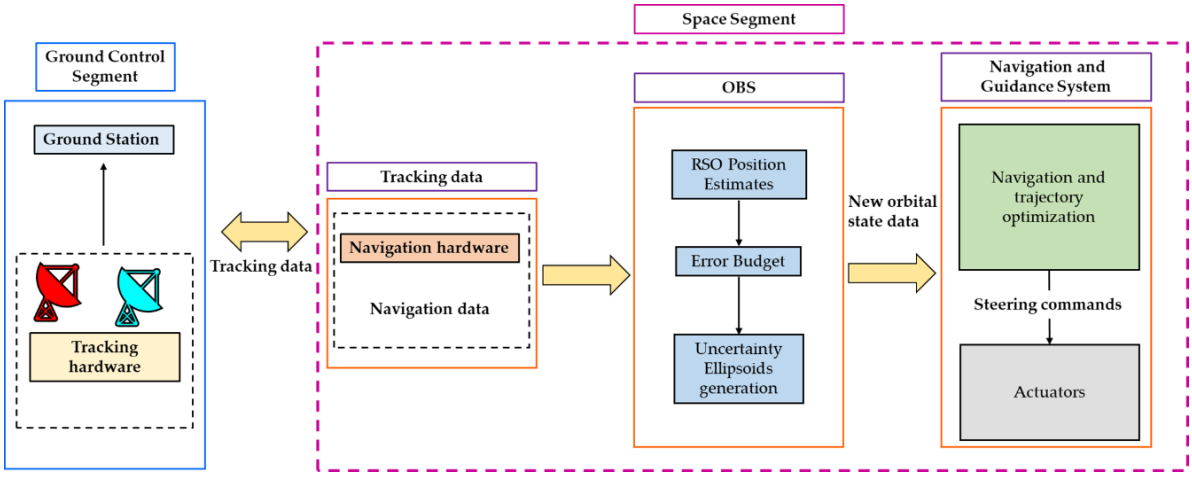

Fig. 4. Collision Avoidance (CA) system architecture.

3. Tracking Algorithm

A single EO sensor cannot directly determine the position of space debris due to its inability to provide range information. In contrast, the position of the RSO can be determined using simultaneous optical measurements from two distinct EO sensors located at two different observation sites, commonly referred to as triangulation [17], [18]. Typically, the EO sensors do not point precisely towards the RSO resulting in an error in the sensor measurement. Triangulation becomes trivial in the absence of measurement error. The current section introduces a suitable tracking algorithm to track the RSO and the corresponding equations required to estimate the position of the RSO, and the errors associated with the measurements. The resulting errors from the triangulation equations are represented in the form of co-variance matrices which are further used to generate the confidence regions around the RSO. The equations that relate the RSO position (x_t ,y_t, z_t) to the sensor positions and the pointing angles that aid the RSO tracking are defined below.

$$x_t = \frac{x_2\tan(\theta_1) - x_1\tan(\theta_2) + (y_1 - y_2)\tan(\theta_1)\tan(\theta_2)}{\tan(\theta_1) - \tan(\theta_2)} \tag{1}$$

$$y_t = \frac{y_1\tan(\theta_1) - y_2\tan(\theta_2) + (x_2 - x_1)}{\tan(\theta_1) - \tan(\theta_2)} \tag{2}$$

$$r_i = \sqrt{(x_i - x_t)^2 + (y_i - y_t)^2} \tag{3}$$

$$z_t = \frac{r_1\tan(\emptyset_1) + z_1 + r_2\tan(\emptyset_2) + z_2}{2} \tag{4}$$

The error propagation equations corresponding to the respective position estimates are derived in [19] with a key assumption that the error generated by each sensor follows Gaussian distribution. The sigmas for each x_t,y_t,z_t are intricate sums of various partial derivatives that are further emphasized in [20].

$$\sigma_{xt} = \sqrt{c_{x,p}^2\sigma_p^2 + \left(rc_{x,\theta}\right)^2\sigma_\theta^2} \tag{5}$$

$$\sigma_{yt} = \sqrt{c_{y,p}^2\sigma_p^2 + \left(rc_{y,\theta}\right)^2\sigma_\theta^2} \tag{6}$$

$$\sigma_{ri} = \sqrt{c_{r,p}^2\sigma_p^2 + \left(rc_{r,\theta}\right)^2\sigma_\theta^2} \tag{7}$$

$$\sigma_{zt} = \sqrt{c_{z,r}^2\sigma_r^2 + \sigma_p^2 + \left(rc_{z,\emptyset}\right)^2\sigma_\emptyset^2} \tag{8}$$

The various c's mentioned in the equations are the error coefficients. For instance, the $c_{x,p}$ indicates the error coefficient for the x coordinate of the target position. $c_{x,\theta,}$ corresponds to error coefficient for azimuth error in x_t. Equations (5)-(8) relate the target position uncertainties to the standard deviation in measurement errors σ_p, σ_θ, σ_φ where σ_p, is the standard deviation in the position measurement, σ_θ is the standard deviation in the azimuth measurement, σ_φ is the standard deviation in the elevation measurement. Equation (8) indicates the error in single sensor measurement of z_t . But since the tracking of the RSO during triangulation is performed using two sensors, the error estimate is calculated as follows:

$$\sigma_{z_t} = \frac{1}{2}\sqrt{\sigma_{z_t}^2(1) + \sigma_{z_t}^2(2) + 2\frac{\partial z_t}{\partial r_1}\frac{\partial z_t}{\partial r_2}Cov(\delta r_1, \delta r_2)} \tag{9}$$

where:
$$Cov(\delta r_1, \delta r_2) = \frac{\partial r_1}{\partial x_t}\frac{\partial r_2}{\partial x_t}\sigma_{x_t}^2 + \frac{\partial r_1}{\partial y_t}\frac{\partial r_2}{\partial y_t}\sigma_{y_t}^2 \tag{10}$$

The steps for obtaining the covariance matrix corresponding to the navigation error are described in detail in the literature[21]. In this case, an on-board GNSS system is assumed to be providing navigational measurements, and the uncertainty magnitudes are derived from an experiment on LEO GPS accuracy published in literature [22]. The co-variance matrix associated with the tracking error can be expressed as:

$$Q_{TRK} = \begin{bmatrix} \sigma_{x_t}^2 & 0 & 0 \\ 0 & \sigma_{y_t}^2 & 0 \\ 0 & 0 & \sigma_{z_t}^2 \end{bmatrix} \tag{11}$$

where the diagonal elements of the matrix defined in (11) are obtained from equations (5), (6), (9). To relate the sensor measurement errors (σ_{p1}, $\sigma_{\theta1}$, $\sigma_{\varphi1}$, σ_{p2}, $\sigma_{\theta2}$, $\sigma_{\varphi2}$) to final RSO position (x_t,y_t,z_t) a total co-variance matrix is developed using the Gauss Helmert formulation [23], [24] where, the vectors of estimated observations and estimated parameters are denoted as *L*, *X* respectively and contain the following elements:

$$L = [x_1, y_1, z_1, \theta_1, \varphi_1, x_2, y_2, z_2, \theta_2, \varphi_2]^{\mathrm{T}} \tag{12}$$

$$X = [x_t, y_t, z_t]^{\mathrm{T}} \tag{13}$$

The co-variance matrix associated with the total error is given by:

$$Q_{TOT(3*3)} = BC_rB^T \tag{14}$$

where C_r is the co-variance matrix of the observations which can be written as a 10*x*10 diagonal matrix with elements (σ_{x1}, $\sigma_{y1,}$ σ_{z1} $\sigma_{\theta1}$, $\sigma_{\varphi1}$, σ_{x2}, $\sigma_{y2,}$ $\sigma_{z2,}$ $\sigma_{\theta2}$, $\sigma_{\varphi2}$). For matrix B the function F (X, L) = 0 is determined as:

$$\begin{aligned} x_t - \frac{x_2\tan(\theta_1) - x_1\tan(\theta_2) + (y_1 - y_2)\tan(\theta_1)\tan(\theta_2)}{\tan(\theta_1) - \tan(\theta_2)} &= 0; \\ y_t - \frac{y_1\tan(\theta_1) - y_2\tan(\theta_2) + (x_2 - x_1)}{\tan(\theta_1) - \tan(\theta_2)} &= 0; \\ z_t - \frac{r_1\tan(\emptyset_1) + z_1 + r_2\tan(\emptyset_2) + z_2}{2} &= 0 \end{aligned} \tag{15}$$

The RSO position estimates and the associated errors are represented as 3D ellipsoids as illustrated in Fig. 5.

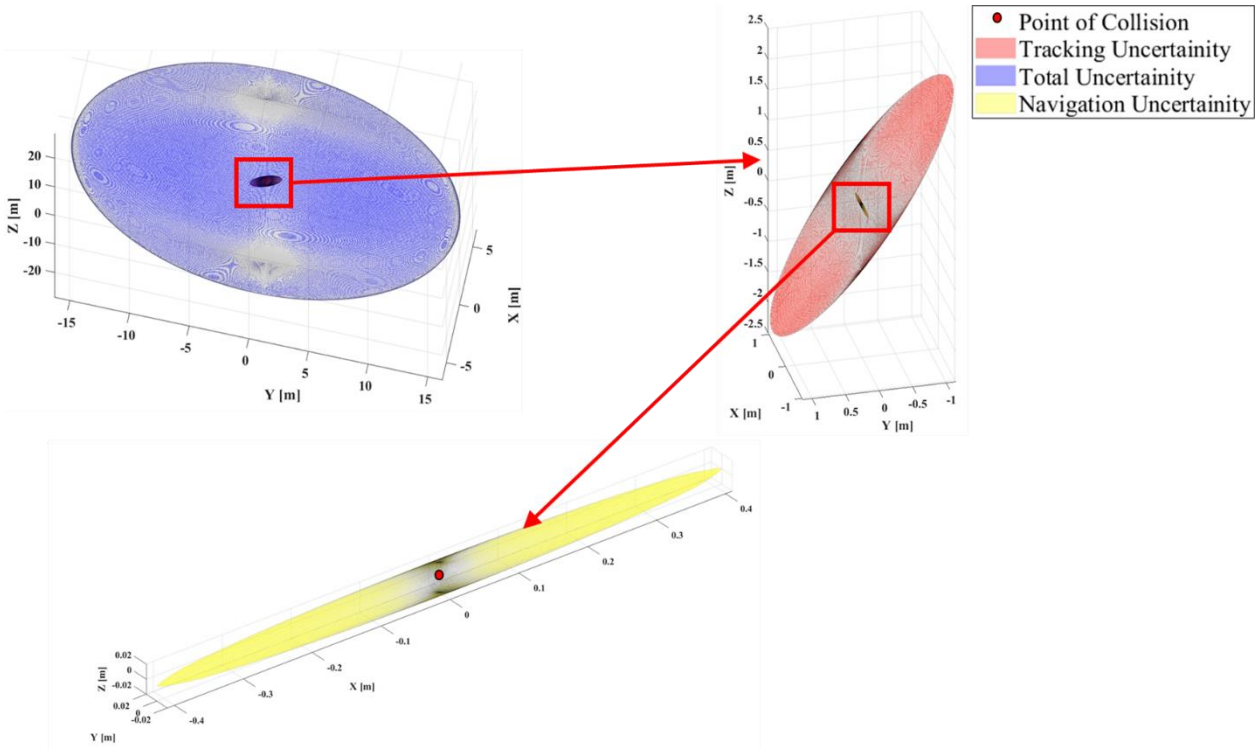

Fig.5. Uncertainty ellipsoids for multi-sensor ground based tracking.

To circumvent the RSO an optimal trajectory is generated using the Particle Swarm Optimization (PSO) algorithm on board the DSS. The PSO technique is chosen as a primary optimization routine due to its ability to achieve global convergence and robustness to solve sophisticated non-linear problems with greater computational efficiency. Additionally, this technique is used widely to solve a plethora of spacecraft trajectory optimization problems and various case studies validate its on-board implementation for adequate convergence time and low computation cost [25], [26]. The particles move iteratively until they converge onto a global optimal solution considering the goal of optimality, minimizing the cost function which describes the quality of the solution and the imposed constraints. The position of the particles iterates according to:

$$X_i^{(k+1)} = X_i^{(k)} + \mathrm{V}_\mathrm{i}^{(\mathrm{k+1})} \tag{16}$$

where V_i^{k+1} is the velocity required to move from k^{th} iteration to $(k+1)^{th}$ iteration, which is given by:

$$V_i^{k+1} = V_i^k + c_1 \cdot r_1 \cdot \left(p_i^k - x_i^k\right) + c_2 \cdot r_2 \cdot \left(p_g^k - x_i^k\right) \tag{17}$$

where:
p_i^k is the best position of particle i at time k;
p_g^k is the global best solution for all particles at time k;
r_1 and r_2 are random numbers between 0 and 1;
c_1 and c_2 are cognitive and scaling parameters respectively and are assigned with a value 2.

Typically, satellite motion in an orbit can be modelled using the classical orbital elements based on Gaussian variational equations. However, these equations result in ambiguity in certain scenarios especially, for the orbits with low eccentricities or inclinations [27]. To avoid this ambiguity a new model is used that employs a set of Modified Equinoctial Parameters (MEE) [28] that comprise of second order zonal harmonics or J_2 perturbation effects (i.e. change in Right Ascension of the Ascending Node (RAAN) and argument of perigee with time), specifically the set of

MEE developed in [29] are employed to solve the low thrust transfer problem. The optimal CA maneuver is chosen based on models that are incorporated into the PSO algorithm[30].

4. Results and discussion

This section emphasizes on the results obtained from the simulation case study in the ground based multi sensor tracking scenario. The RSO position estimates are obtained using the tracking algorithm in section 3. The tracking algorithm takes the sensor positions in a cartesian frame as inputs which are tabulated in Table 2.

Table 2. Sensor coordinates in cartesian frame with Earth as centre.

Cartesian co-ordnates	X_i (km)	Y_i(km)	Z_i (km)	Azimuth (deg)	Elevation (deg)
Sensor 1	1880.82	13.78	6221.92	30	60
Sensor 2	6503.13	114.64	595.35	315	65

The RSO position estimates and the associated errors are tabulated in Table 3.

Table 3. RSO position estimates and associated errors.

Parameter	X_t (km)	Y_t (km)	Z_t (km)	Range (km)
RSO position	3609.6	3008.1	10791	3774.8
Error	6.5	10.24	28.7	9.38

The uncertainties tabulated in Table 3 are represented as confidence regions or uncertainty ellipsoids corresponding to navigation, tracking and total uncertainties around the RSO in Figure 5. The satellite identified with high risk of collision performs a collision avoidance maneuver to reorient its initial orbit to a modified orbit with a semimajor axis increased to 6.5 km to avoid the uncertainty volume. The initial orbital parameters before the CA manoeuvre and final orbital parameters after the manoeuvre is tabulated in Table 4. It is assumed that the spacecraft that performs the orbit raising maneuver is equipped with Nano Avionics: EPSSC1 thruster that can generate a thrust of 1N and specific impulse of 213 seconds [31].

Table 4. Initial and Final orbital parameters of the DSS satellite.

Orbital parameter	Initial state	Final state
a (km)	6828	6834.4
e	0.002	0.002
i (deg)	95	95
ω(deg)	30	30
Ω (deg)	0	0

The change in trajectory due to CA manoeuvre is illustrated in Fig.6b and the control parameters for the constant thrust directions illustrated in Fig. 6a are tabulated in Table 5. The MATLAB solver provides the result after 351,000 iterations with a total run rime of 1922.8 seconds on an Intel Core i7 7th generation processor.

Table 5. Control parameters for CA manoeuvre.

t_f (min)	α_M (deg)	β_M (deg)	f_T	k_T (rad)	p_1	p_2
28.75	-2.6	-2.47	0.5	0.176	0.115	1.06

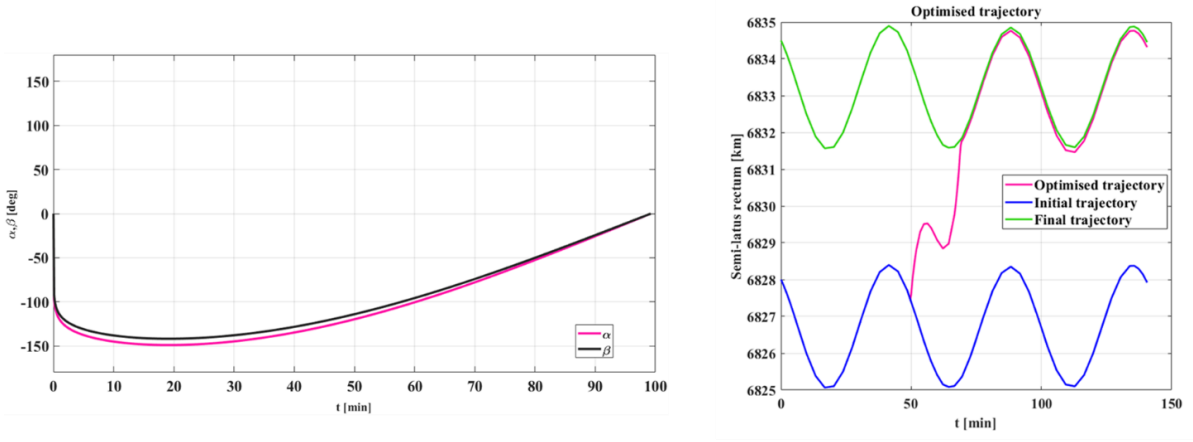

(a) **(b)**

Fig.6. (a) Change of thrust vector angles in time; (b) Change in DSS trajectory with respect to time.

5. Conclusion

The research presented in this article addressed multi-sensor Resident Space Object (RSO) tracking using ground based optical sensors in the context of Space Domain Awareness (SDA) for Space Traffic Management (STM). Single Electro-Optical sensor (EO) is insufficient for tracking RSO due to lack of range information. In contrast, performing triangulation using simultaneous measurements from multiple ground based optical sensors solves the tracking problem significantly. The proposed algorithm results in RSO position estimation along with the associated error budget which is further quantified into 3D uncertainty volumes/confidence regions. Following this, the DSS satellite can perform a CA maneuver to circumvent the RSO. A simulation case study is presented, and the results substantiate the validity of the proposed mathematical framework. Current research is addressing the development of Artificial Intelligence (AI)-based autonomous navigation/guidance algorithms and integration of SBSS and ground-based tracking sensors towards maximizing DSS performance in different applications and operational conditions. The combined use of these technologies facilitates a high level of spacecraft autonomy (trusted autonomy) which is an important objective for future space missions.

References

[1] S. Mullick, Y. Srinivasa, A. K. Sahu, and J. T. Sata, "A Comprehensive Study on Space Debris, Threats Posed by Space Debris, and Removal Techniques," *SSRN Electron. J.*, 2019, doi: 10.2139/ssrn.3511445.

[2] "Space Environment Statistics · Space Debris User Portal." https://sdup.esoc.esa.int/discosweb/statistics/ (accessed Jul. 16, 2022).

[3] jbaker, "Space traffic management: Time for action," *Atlantic Council*, Aug. 02, 2022. https://www.atlanticcouncil.org/in-depth-research-reports/issue-brief/space-traffic-management-time-for-action/ (accessed Jan. 22, 2023).

[4] S. Hilton, R. Sabatini, A. Gardi, H. Ogawa, and P. Teofilatto, "Space traffic management: towards safe and unsegregated space transport operations," *Prog. Aerosp. Sci.*, vol. 105, pp. 98–125, Feb. 2019, doi: 10.1016/j.paerosci.2018.10.006.

[5] M. R. Ackermann, R. Kiziah, P. C. Zimmer, J. McGraw, and D. Cox, "A systematic examination of ground-based and space-based approaches to optical detection and tracking of satellites," in *31st Space Symposium*, 2015.

[6] H. Klinkrad, *Space debris: models and risk analysis*. Berlin ; New York : Chichester, UK: Springer ; Published in association with Praxis Pub, 2006.

[7] E. Lee, S.-Y. Park, H. Hwang, J. Choi, S. Cho, and J. H. Jo, "Initial orbit association and long-term orbit prediction for low earth space objects using optical tracking data," *Acta Astronaut.*, vol. 176, pp. 247–261, 2020, doi: https://doi.org/10.1016/j.actaastro.2020.06.046.

[8] T. Schildknecht *et al.*, "Optical observations of space debris in GEO and in highly-eccentric orbits," *Adv. Space Res.*, vol. 34, no. 5, pp. 901–911, 2004, doi: https://doi.org/10.1016/j.asr.2003.01.009.

[9] T. Schildknecht, "Optical surveys for space debris," *Astron. Astrophys. Rev.*, vol. 14, no. 1, pp. 41–111, Jan. 2007, doi: 10.1007/s00159-006-0003-9.

[10] T. Schildknecht, U. Hugentobler, and A. Verdun, "Optical observations of space debris with the Zimmerwald 1-meter telescope," *Adv. Space Res.*, vol. 19, no. 2, pp. 221–228, 1997, doi: https://doi.org/10.1016/S0273-1177(97)00004-5.

[11] R. Sabatini, M. Battipede, and F. Cairola, "Innovative Techniques for Spacecraft Separation Assurance and Debris Collision Avoidance," 2020.

[12] S. Hilton, F. Cairola, A. Gardi, R. Sabatini, N. Pongsakornsathien, and N. Ezer, "Uncertainty quantification for space situational awareness and traffic management," *Sensors*, vol. 19, no. 20, p. 4361, 2019.

[13] K. Hussain, K. Hussain, S. Carletta, and P. Teofilatto, *Deployment of a microsatellite constellation around the Moon using chaotic multi body dynamics*. 71st International Astronautical Congress (IAC), Dubai, United Arab Emirates, 2021.

[14] K. Thangavel, D. Spiller, R. Sabatini, P. Marzocca, and M. Esposito, "Near Real-time Wildfire Management Using Distributed Satellite System," *IEEE Geosci. Remote Sens. Lett.*, pp. 1–1, 2022, doi: 10.1109/LGRS.2022.3229173.

[15] D. Spiller, K. Thangavel, S. T. Sasidharan, S. Amici, L. Ansalone, and R. Sabatini, "Wildfire segmentation analysis from edge computing for on-board real-time alerts using hyperspectral imagery," in *2022 IEEE International Conference on Metrology for Extended Reality, Artificial Intelligence and Neural Engineering (MetroXRAINE)*, Rome, Italy, Oct. 2022, pp. 725–730. doi: 10.1109/MetroXRAINE54828.2022.9967553.

[16] K. Thangavel *et al.*, "Autonomous Satellite Wildfire Detection Using Hyperspectral Imagery and Neural Networks: A Case Study on Australian Wildfire," *Remote Sens.*, vol. 15, no. 3, p. 720, Jan. 2023, doi: 10.3390/rs15030720.

[17] L. Chen, C. Liu, Z. Li, and Z. Kang, "A New Triangulation Algorithm for Positioning Space Debris," *Remote Sens.*, vol. 13, no. 23, p. 4878, Dec. 2021, doi: 10.3390/rs13234878.

[18] J. N. Sanders-Reed, "Impact of tracking system knowledge on multisensor 3D triangulation," presented at the AeroSense 2002, Orlando, FL, Jul. 2002, pp. 33–41. doi: 10.1117/12.472599.

[19] J. N. Sanders-Reed, "Error propagation in two-sensor three-dimensional position estimation," *Opt. Eng.*, vol. 40, no. 4, pp. 627–636, 2001.

[20] J. N. Sanders-Reed, "Triangulation Position Error Analysis for Closely Spaced Imagers," presented at the SAE 2002 World Congress & Exhibition, Mar. 2002, pp. 2002-01–0685. doi: 10.4271/2002-01-0685.

[21] S. Hilton, F. Cairola, A. Gardi, R. Sabatini, N. Pongsakornsathien, and N. Ezer, "Uncertainty quantification for space situational awareness and traffic management," *Sensors*, vol. 19, no. 20, p. 4361, 2019.

[22] I. GNSS, "GPS Receiver Performance On Board a LEO Satellite," *Inside GNSS - Global Navigation Satellite Systems Engineering, Policy, and Design*, Jul. 21, 2014. https://insidegnss.com/gps-receiver-performance-on-board-a-leo-satellite/ (accessed Oct. 07, 2022).

[23] G. R. Curry, "radar System Performance Modeling, ARTECH HOUSE," *Inc Ed Norwood MA USA*, 2005.

[24] D. A. Vallado, *Fundamentals of astrodynamics and applications*, vol. 12. Springer Science & Business Media, 2001.

[25] M. Lin, Z.-H. Zhang, H. Zhou, and Y. Shui, "Multiconstrained Ascent Trajectory Optimization Using an Improved Particle Swarm Optimization Method," *Int. J. Aerosp. Eng.*, vol. 2021, 2021.

[26] A. Rahimi, K. Dev Kumar, and H. Alighanbari, "Particle Swarm Optimization Applied to Spacecraft Reentry Trajectory," *J. Guid. Control Dyn.*, vol. 36, no. 1, pp. 307–310, 2013, doi: 10.2514/1.56387.

[27] J. T. Betts, *Practical Methods for Optimal Control and Estimation Using Nonlinear Programming, Second Edition*. Society for Industrial and Applied Mathematics, 2010. doi: 10.1137/1.9780898718577.

[28] G. Baù, J. Hernando-Ayuso, and C. Bombardelli, "A generalization of the equinoctial orbital elements," *Celest. Mech. Dyn. Astron.*, vol. 133, no. 11, pp. 1–29, 2021.

[29] S. Eves, "Applied Nonsingular Astrodynamics: Optimal Low-Thrust Orbit Transfer J. A. Kéchichian Cambridge University Press, University Printing House, Shaftesbury Road, Cambridge CB2 8BS, UK. 2018. xvii; 461 pp.

ISBN 978-1-108-47236-4.," *Aeronaut. J.*, vol. 124, no. 1282, pp. 2036–2037, Dec. 2020, doi: 10.1017/aer.2020.105.

[30] E. Lagona, S. Hilton, A. Afful, A. Gardi, and R. Sabatini, "Autonomous Trajectory Optimisation for Intelligent Satellite Systems and Space Traffic Management," *Acta Astronaut.*, vol. 194, pp. 185–201, May 2022, doi: 10.1016/j.actaastro.2022.01.027.

[31] "CubeSat Propulsion System EPSS," *NanoAvionics*. https://nanoavionics.com/cubesat-components/cubesat-propulsion-system-epss/ (accessed Jan. 02, 2023).